

---

# Exploiting the Asymmetric Uncertainty Structure of Pre-trained VLMs on the Unit Hypersphere

---

Li Ju<sup>\*†</sup> Max Andersson<sup>†</sup> Stina Fredriksson<sup>†</sup> Edward Glöckner<sup>†</sup>

Andreas Hellander<sup>†</sup> Ekta Vats<sup>†</sup> Prashant Singh<sup>‡‡</sup>

## Abstract

Vision-language models (VLMs) as foundation models have significantly enhanced performance across a wide range of visual and textual tasks, without requiring large-scale training from scratch for downstream tasks. However, these deterministic VLMs fail to capture the inherent ambiguity and uncertainty in natural language and visual data. Recent probabilistic post-hoc adaptation methods address this by mapping deterministic embeddings onto probability distributions; however, existing approaches do not account for the asymmetric uncertainty structure of the modalities, and the constraint that meaningful deterministic embeddings reside on a unit hypersphere, potentially leading to suboptimal performance. In this paper, we address the asymmetric uncertainty structure inherent in textual and visual data, and propose AsymVLM to build probabilistic embeddings from pre-trained VLMs on the unit hypersphere, enabling uncertainty quantification. We validate the effectiveness of the probabilistic embeddings on established benchmarks, and present comprehensive ablation studies demonstrating the inherent nature of asymmetry in the uncertainty structure of textual and visual data.

## 1 Introduction

Vision-language models (VLMs) have demonstrated impressive capabilities in understanding visual and linguistic information, by constructing a joint embedding space that aligns image and text embeddings [4, 29]. Models like CLIP [17] and BLIP [13], enable a wide range of downstream applications, such as zero-shot classification [1], image-to-text retrieval [5], optical character recognition [26]. However, due to the inherent ambiguity within text and image data, aligned point estimates for text and image embeddings produced by deterministic VLMs may not fully capture the complex relationships between the visual and linguistic embedding spaces.

Alternatively, instead of learning deterministic point estimate embeddings, probabilistic embedding methods [8] map text and language data onto probability distributions, more effectively capturing the ambiguity and uncertainty of the data. However, they entail training probabilistic VLMs from scratch on massive datasets – an expensive process that forgoes the strengths of established deterministic VLMs. To explore post-hoc methods for constructing probabilistic embeddings from pretrained deterministic VLMs, recent frameworks such as ProbVLM [24] and BayesVLM [3] have been proposed. However, the ambiguous nature of text-to-image retrieval is due to both textual abstraction and image variability, while image-to-text ambiguity arises from the multiplicity of textual descriptions. Existing methods overlook this asymmetric nature in texts and images, and the fact that the embeddings of most pre-trained VLMs reside on a unit hypersphere, instead of the Euclidean space.

<sup>\*</sup>Corresponding author (li.ju@it.uu.se)

<sup>†</sup>Department of Information Technology, Uppsala University, Uppsala, Sweden

<sup>‡</sup>Science for Life Laboratory, Uppsala University, Uppsala, Sweden

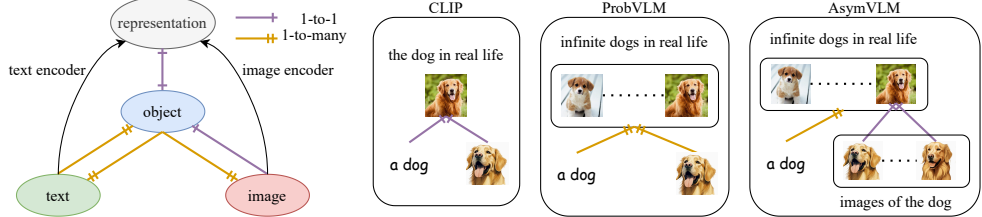


Figure 1: **Left:** Mapping relations between text, image, object, and representation spaces. **Right:** Comparison of methods – CLIP uses deterministic one-to-one mappings; ProbVLM introduces one-to-many mappings via probabilistic embeddings; AsymVLM further captures asymmetry structure between texts, images and objects.

In this work, we propose a post-hoc method, Asymmetric Probabilistic Vision-Language Model (AsymVLM), to model the uncertainty of embeddings obtained from pretrained VLMs. We first formulate the problem of constructing vision-language models, and tackle the asymmetric structure of texts and image in Section 3. The proposed method AsymVLM is derived in Section 4. In Section 5, we evaluate the quality of the uncertainty estimates, conduct an ablation study to validate our hypotheses, and further demonstrate the potential applications of the proposed method. We present concluding remarks, and discuss limitations and future directions of the work in Section 6.

## 2 Related work

**Vision-language models** Recent advancements in vision-language modeling have facilitated the development of multimodal models capable of learning a shared embedding space for images and text. These models typically achieve this by optimizing directional similarity metrics, such as cosine similarity. Notable works including CLIP [17], BLIP [13], SigLip [28], typically align paired image-text representations by maximizing the cosine similarity between corresponding embeddings. This strategy has proven to be effective for large-scale training, enabling these models to capture semantic relationships, and generalize well across diverse downstream tasks. However, these pretrained VLMs offer deterministic mappings that fail to capture the inherent ambiguity in the inputs.

**Probabilistic VLMs** Methods have been proposed to improve deterministic VLM embeddings by learning a unified probabilistic embedding space for both visual and textual data. Methods such as PCME [8], and PFE [23] learn to map texts and images to aligned probability distributions, by maximizing the cross-modal likelihood between corresponding text and image data. However, these approaches require training from scratch, which is computationally expensive as existing high-quality deterministic VLMs are not fully leveraged. A more resource-efficient alternative is the probabilistic adaptation of pretrained VLMs. ProbVLM [24] trains an adapter to construct probability distributions from deterministic embeddings, while BayesVLM [3] estimates the uncertainty of cosine similarity through post-hoc Bayesian posterior approximation. As mentioned in Section 1 (and detailed in the following Section), although having demonstrated their efficacy for uncertainty quantification, existing post-hoc approaches do not consider the asymmetry in uncertainty structures between textual and visual data, and the constraint that meaningful embeddings of most pretrained VLMs reside on the unit sphere, resulting in sub-optimal performance.

**Embeddings on the unit hypersphere** Cosine similarity is widely utilized in contemporary VLMs and foundation models pre-trained with contrastive loss [6, 17, 7]. This approach inherently constrains the learned embeddings to reside on the unit hypersphere. These embeddings have been shown to have advantages such as improved uniformity and alignment compared to their Euclidean counterparts [25]. Beyond cosine similarity, embeddings on the unit hypersphere can also be explicitly modeled by assuming directional distributions, such as the von Mises-Fisher (vMF) distribution [10]. Scott et al. [20] introduced a contrastive loss based on the vMF distribution as a pretraining method, while [19] proposes a method to distill pretrained VLMs, adapting student models with vMF assumptions for zero-shot classification. However, while these approaches focus on improving empirical performance in downstream tasks, none explicitly model the uncertainty of embeddings from pretrained VLMs.

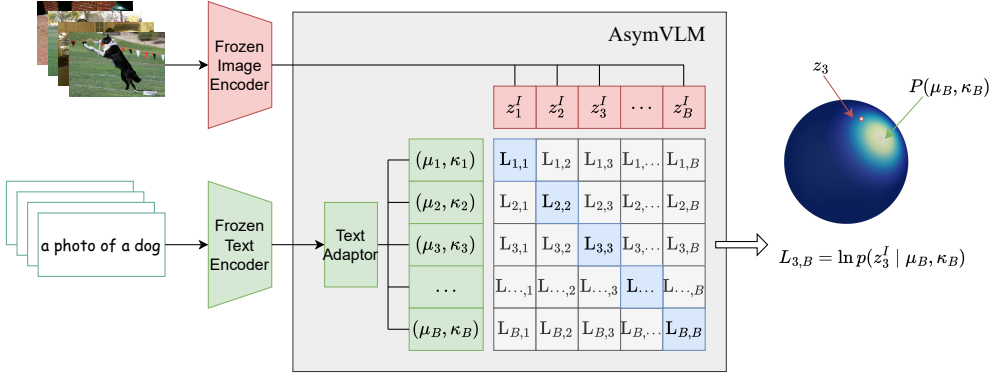


Figure 2: Asymmetric probabilistic adaptation (AsymVLM): Texts are encoded with a frozen text encoder and adaptor to produce probabilistic hyperspherical embeddings (e.g., vMF distribution), while image are deterministically encoded via a frozen image encoder. The log likelihood matrix  $L$ , with element  $L_{m,n}$  representing the log likelihood of image vector  $z_n^I$  given text embedding  $z_m^T \sim P(\mu_m, \kappa_m)$ , is optimized using InfoNCE to maximize diagonals and minimize off-diagonals.

### 3 Asymmetric structure of texts and images

In linguistics and semiotics, the relationship between words and objects is often described as the type–token-distinction [27]: the word "dog" is a type (an abstract label applicable to any dog), whereas a single dog is a token (a specific instance). Textual labels are high-level abstractions, and can map onto infinitely many unique physical examples. In contrast, a single dog is one particular realization of the word "dog". However, for the single dog, infinitely many images can be taken with different setups, e. g., different angles, color tones. The one-to-many and many-to-one mappings from the text and vision to physical world, respectively, imply the intrinsic asymmetric structure in textual and visual information. This is of vital importance for the understanding cross-modal retrieval, and subsequently the building of VLMs.

#### 3.1 Mathematical formulation

Let  $\mathcal{T}$ ,  $\mathcal{I}$ ,  $\mathcal{O}$  and  $\tilde{\mathcal{O}}$  denote the text, image, (real-world) object and (numerical) representation space respectively. The relationships between  $t \in \mathcal{T}$ ,  $i \in \mathcal{I}$ ,  $o \in \mathcal{O}$  and  $\tilde{o} \in \tilde{\mathcal{O}}$  can be presented as follows.

MAPPING	DEFINITION / DERIVATION	ONE-TO-MANY?
Text $\rightarrow$ Object	$\Phi_T(t) := \{o \in \mathcal{O} : o \text{ can be described by } t\}$	✓
Object $\rightarrow$ Image	$\Phi_I(o) := \{i \in \mathcal{I} : i \text{ is an image of } o\}$	✓
Text $\rightarrow$ Image	$(\Phi_I \circ \Phi_T)(t) = \bigcup_{o \in \Phi_T(t)} \Phi_I(o)$	✓
Image $\rightarrow$ Object	$\Phi_I^{-1}(i) := o$	✗(assumption)
Object $\rightarrow$ Text	$\Phi_T^{-1}(o) := \{t \in \mathcal{T} : o \text{ can be described by } t\}$	✓
Image $\rightarrow$ Text	$(\Phi_T^{-1} \circ \Phi_I^{-1})(i) = \{t \in \mathcal{T} : \Phi_I^{-1}(i) \in \Phi_T(t)\}$	✓
Object $\leftrightarrow$ Representation	$\psi(o) := \tilde{o}$ , $\psi^{-1}(\tilde{o}) = o$	✗
Text encoder	$f_T \approx \psi \circ \Phi_T$	✓
Image encoder	$f_I \approx \psi \circ \Phi_I^{-1}$	✗

**Building VLMs** Existing datasets such as MS-COCO [14] and Flickr30K [16] collect data in the form of  $\{(t_n, i_n)\}_{n=1}^N$  such that there exist  $o_n \in \mathcal{O}$  which satisfies  $o_n \in \Phi_T(t_n)$  and  $i_n \in \Phi_I(o_n)$ . Based on such datasets, we aim to find a  $d$ -dimensional real-valued representation space  $\tilde{\mathcal{O}} \subset \mathbb{R}^d$ , such that there exists a bijective function  $\psi : \mathcal{O} \rightarrow \tilde{\mathcal{O}}$ . More importantly, the goal is to approximate the composite function  $\psi \circ \Phi_T : \mathcal{T} \rightarrow \mathcal{P}(\tilde{\mathcal{O}})$  and  $\psi \circ \Phi_I^{-1} : \mathcal{I} \rightarrow \tilde{\mathcal{O}}$  with finite samples from datasets as the text encoder  $f_T$  and image encoder  $f_I$ , following the Platonic representation hypothesis [11].

### 3.2 Motivating the approach

Trained on datasets in the form of  $\{(t_n, i_n)\}_{n=1}^N$ , existing deterministic pre-trained models maximize the similarity measure between matching text-image pairs while minimizing it for non-matching pairs [17, 28]. These approaches effectively learn a real-valued embedding space  $\tilde{\mathcal{O}}$ , along with deterministic text and image encoders. Existing probabilistic adaptation methods, rather than mapping an image or caption to a single point in the embedding space, represent elements of  $\mathcal{T}$  or  $\mathcal{I}$  as random variables in  $\tilde{\mathcal{O}}$ , thereby capturing the inherent one-to-many nature of the relationships.

However, the relationships among texts, images, and objects are inherently asymmetric, leading to distinct structures in text-to-image and image-to-text retrieval tasks. While both tasks are one-to-many, the asymmetry arises from different sources: abstraction and visual variability in text-to-image versus diverse textual descriptions in image-to-text. This structural difference motivates the use of asymmetric probabilistic structure for encoders within the representation space.

*From the uncertainty quantification (UQ) perspective*, aleatoric uncertainty arises from inherent randomness that cannot be reduced by additional data, while epistemic uncertainty stems from the model’s limited knowledge. Text carries high aleatoric uncertainty because a single label (e.g., “a dog”) can refer to countless variations – details like breed, size, or context being ambiguous. In contrast, images usually depict specific objects or scenes; a well-trained model can precisely identify them, given ample examples. However, if the training data lacks diversity, the model’s epistemic uncertainty about an image will remain high, while aleatoric uncertainty will inherently be low.

Assuming an underlying asymmetric uncertainty structure, a direction for improvement emerges. For text embeddings, it is essential to capture the wide variance inherent in language via distributions to reflect the multitude of corresponding objects. Conversely, image embeddings can be modeled deterministically and the uncertainty is reduced through large coverage of visual data in the datasets.

## 4 Method

With a pretrained VLM such as CLIP or SigLip, we denote the text encoder as  $f_T : \mathcal{T} \rightarrow \mathbb{S}^{d-1}$  and image encoder as  $f_I : \mathcal{I} \rightarrow \mathbb{S}^{d-1}$ , where  $d$  is the dimension of the representation space.

### 4.1 Asymmetric probabilistic adaptation

As discussed in Section 3, capturing the variance is crucial for text embeddings, while ensuring coverage in training data is key for image embeddings. To achieve this, we introduce a text adapter  $g_T$  for the text encoder  $f_T$ , while retaining the deterministic embeddings from the image encoder  $f_I$ , as expanding image data coverage lies beyond the scope of this work. Formally, the embedding of any text  $t \in \mathcal{T}$  is modeled by a random variable  $z^T$ ,

$$z^T \sim P(\theta(t)) \text{ where } \theta(t) := g_T \circ f_T(t), \quad (1)$$

where  $P(\theta(t))$  denotes a distribution parametrized by  $\theta(t)$  predicted by a neural network given corresponding text. The deterministic image embedding  $z^I$  from the image encoder  $f_I$  is retained.

**Objective function** For any batch of data  $\{(t_1, i_1), \dots, (t_B, i_B)\}$ , we aim to maximize  $\ln p_{z_n^T}(z_n^T)$  for all  $n \in [B]$  while minimizing  $\ln p_{z_m^T}(z_n^I)$  for all  $n, m \in [B], n \neq m$ , where  $p_a(b)$  denotes the value of the PDF of random variable  $a$  at  $b$ . First we define the log likelihood matrix  $L \in \mathbb{R}^{B \times B}$ , where the  $(m, n)$ -th element is computed as  $L(m, n) = \ln p_{z_m^T}(z_n^I)$ , for  $n, m \in [B]$ .

To maximize the diagonal elements and minimize the off-diagonal elements of  $L$ , we apply the InfoNCE loss to  $L$  and obtain the objective function to be minimized,

$$\arg \min_{\theta \in \Theta} -\frac{1}{2B} \sum_{n=1}^B \left[ \ln \frac{\exp(\tau \cdot L(n, n))}{\sum_{m=1}^B \exp(\tau \cdot L(n, m))} + \ln \frac{\exp(\tau \cdot L(n, n))}{\sum_{m=1}^B \exp(\tau \cdot L(m, n))} \right], \quad (2)$$

where  $\tau$  is a temperature parameter and  $\theta$  is the parameter set of distribution  $P_{z^T}(\theta(t))$ .

## 4.2 Modelling on the unit hypersphere

The shared representation space built by most pre-trained VLMs is  $\mathbb{S}^{d-1}$ , the domain in which both  $\mathbf{z}^T$  and  $\mathbf{z}^I$  reside. This observation necessitates the selection of a directional distribution for  $P(\theta(t))$ , defined on  $\mathbb{S}^{d-1}$ . To properly construct a probabilistic embedding on  $\mathbb{S}^{d-1}$ , directional distributions for the embeddings should be employed – either projected distributions (e.g., the angular normal distribution) or native directional distributions (e.g., the vMF distribution). In this work, we use the vMF, and power spherical (PS) distributions to model the text embeddings distribution. The former is generally considered as the simplest directional distribution, while the latter is reported to be an alternative to the vMF distribution with a closed form normalization constant.

**Derivation w.r.t. vMF distribution** The vMF distribution  $\text{vMF}(\mu, \kappa)$  is a probability distribution on  $\mathbb{S}^{d-1}$ , parameterized by a mean direction  $\mu \in \mathbb{R}^d$  and an isotropic concentration parameter  $\kappa \in \mathbb{R}$ , where  $\|\mu\|_2 = 1$  and  $\kappa \geq 0$ . The PDF for random unit vector  $x$  is given by,

$$p(x; \mu, \kappa) = C_d(\kappa) \exp(\kappa \cdot \mu^\top x), \text{ where } C_d(\kappa) = \frac{\kappa^{d/2-1}}{(2\pi)^{d/2} I_{d/2-1}(\kappa)},$$

and  $I_p$  denotes the modified Bessel function of the first kind, at order  $p$ .

Following Equation 1, assuming that  $\mathbf{z}^T \sim \text{vMF}(\mu(t), \kappa(t))$  for text  $t \in \mathcal{T}$ , for any image  $i \in \mathcal{I}$ , we have  $\ln p_{\mathbf{z}^T}(\mathbf{z}^I) = \kappa \cdot \mu(t)^\top \mathbf{z}^I + \ln C_d(\kappa(t))$ . However, computing  $C_d(\kappa)$  is intractable in the high dimensional space, yet [20] have shown that  $\ln C_d(\kappa)$  can be approximated by  $F_d(\kappa) + \text{const.}$ , where  $F_d(\kappa)$  is given by,

$$\begin{aligned} F_d(\kappa) = & \frac{d-1}{4} \ln \left( \frac{d-1}{2} + \sqrt{\left( \frac{d-1}{2} \right)^2 + \kappa^2} \right) - \frac{1}{2} \sqrt{\left( \frac{d-1}{2} \right)^2 + \kappa^2} \\ & + \frac{d-1}{4} \ln \left( \frac{d-1}{2} + \sqrt{\left( \frac{d+1}{2} \right)^2 + \kappa^2} \right) - \frac{1}{2} \sqrt{\left( \frac{d+1}{2} \right)^2 + \kappa^2}. \end{aligned}$$

Injecting the log likelihood of vMF into Equation 2 results in the vMF kernel for the objective function  $L_{\text{vMF}}$  as follows,

$$L_{\text{vMF}}(r, s) = \kappa(t_r) \cdot \mu(t_r)^\top \mathbf{z}_s^I + F_d(\kappa(t_r)), \quad \forall r, s \in [B].$$

The detailed derivation for the approximation is deferred to Appendix A.1.

**Derivation w.r.t. PS distribution** The power spherical distribution  $\text{PS}(\mu, \kappa)$  is an alternative to vMF, also parametrized by a mean direction  $\mu \in \mathbb{R}^d$  and a concentration parameter  $\kappa \in \mathbb{R}$  with  $\|\mu\|_2 = 1$  and  $\kappa \geq 0$ . The PDF of a PS distribution is given by,

$$p(x; \mu, \kappa) = (1 + \mu^\top x)^\kappa \cdot C_d(\kappa), \text{ where } C_d(\kappa) = \left\{ 2^{\alpha+\beta} \pi^\beta \frac{\Gamma(\alpha)}{\Gamma(\alpha+\beta)} \right\}^{-1},$$

and  $\alpha = (d-1)/2 + \kappa$ ,  $\beta = (d-1)/2$ .

Similarly, following Equation 1, assuming that  $\mathbf{z}^t \sim \text{PS}(\mu(t), \kappa(t))$  for text  $t \in \mathcal{T}$ , for any image  $i \in \mathcal{I}$ , injecting the log likelihood of PS distribution in Equation 2 results in the PS kernel  $L_{\text{PS}}$ ,

$$\begin{aligned} L_{\text{PS}}(r, s) = & \kappa(t_r) \ln(1 + \mu(t_r)^\top \mathbf{z}_s^I) - (d-1 + \kappa(t_r)) \ln 2 \\ & - \ln \Gamma \left( \frac{d-1}{2} + \kappa(t_r) \right) + \ln \Gamma(d-1 + \kappa(t_r)), \quad \forall r, s \in [B]. \end{aligned}$$

## 4.3 Connections to CLIP

Equation 2 can be rewritten in the following form,

$$\theta = \arg \min_{\theta \in \Theta} - \frac{1}{2B} \sum_{n=1}^B \left[ \ln \frac{\exp(\tau \delta(n, n))}{\sum_{m=1}^B \exp(\tau \ln \delta(n, m))} + \ln \frac{\exp(\tau \delta(n, n))}{\sum_{m=1}^B \exp(\tau \delta(m, n))} \right].$$

Denoting  $\text{CosSim}(r, s) = \mu(t_r)^\top z_s^I$ , for any  $r, s \in [B]$  we have,

$$\begin{aligned} \text{for CLIP: } \delta_{\text{CLIP}}(r, s) &= \text{CosSim}(r, s), \\ \text{for AsymVLM}_{\text{vMF}}: \delta_{\text{vMF}}(r, s) &= \kappa(t_r) \cdot \text{CosSim}(r, s) + F_d(\kappa(t_r)), \\ \text{for AsymVLM}_{\text{PS}}: \delta_{\text{PS}}(r, s) &= \kappa(t_r) \ln(1 + \text{CosSim}(r, s)) + \ln C_d(\kappa(t_r)). \end{aligned} \quad (3)$$

Given that  $\kappa(t_r) \geq 0$ , it is clear that the latter two objectives are monotonically increasing w.r.t.  $\delta_{\text{CLIP}}$  with an additional parameter  $\kappa$ . These can be interpreted as *extensions of the CLIP loss by introducing  $\kappa$ , the concentration parameter, to model the variance of the text embedding without drifting from the pre-trained models using cosine similarities*.

Equation 3 demonstrates AsymVLM’s consistency with the underlying ideas of CLIP, while incorporating mechanisms to account for embedding variance. AsymVLM ultimately offers a more refined and probabilistically grounded approach to modeling semantic relationships between text and images. Furthermore, AsymVLM can be extended to a SigLip variant. Inference using AsymVLM also extends beyond simply computing the cosine similarity, to utilizing the maximum likelihood principle, with a clearer statistical explanation. Details about the inference process and its SigLip-variant are provided in Appendix A.2 and A.3.

## 5 Empirical results

We compare AsymVLM to the baselines on benchmark datasets, and subsequently present an ablation study. Further, extended analyses and demonstration on two downstream applications are presented.

**Datasets, baselines and metrics** The MS-COCO [14] and Flickr-30k [16] datasets are used to train the adapters. Additionally, a subset of the Conceptual Caption dataset [22] of 200k samples (CC-200k) is also used. To understand the nature of learned uncertainty, the HierarCap dataset [2] is used, containing four captions of different abstraction levels for each image. The baselines include ProbVLM, PFE and PCME++ adapted from pretraining methods (denoted by PFE\* and PCME++\*, respectively). BayesVLM is excluded from the baselines as it does not provide a single scalar quantifying embedding uncertainty, but propagates scalar uncertainty over cosine similarities. The pre-trained VLM used in the experiments in the main text is CLIP (ViT-B/32 backbone). We assess the uncertainty quality in text embeddings by evaluating recall@1 performance in cross-modal retrieval tasks. A strong positive correlation between uncertainty and errors indicates that higher uncertainty leads to poorer embeddings and lower recall. For each task, we group results by uncertainty levels and compute Spearman’s rank correlation ( $S$ ) between uncertainty and recall [21]. We then fit a regressor ( $R^2$ ) to determine if the performance drop is linear, and compare average Recall@1 across uncertainty levels for different methods. All experiments were repeated *five times with different random seeds*, and we report the mean results with full standard deviations provided in the Appendix.

### 5.1 Evaluation of UQ and cross-modal retrieval

Figure 3 and Table 1 summarize the main results comparing the proposed AsymVLM with baseline methods. For uncertainty quantification, results indicate that while all methods capture text uncertainty to some degree, AsymVLM consistently outperforms its counterparts. As the uncertainty level increases, AsymVLM is the only method for which Recall@1 decreases strictly monotonically. Moreover, AsymVLM also meets or exceeds competing approaches on both  $R^2$  and  $S$  scores.

In cross-modal retrieval, AsymVLM<sub>VMF</sub> and AsymVLM<sub>PS</sub> achieve the highest and second-highest Recall@1 scores across all datasets. Note that the retrieval performances of PFE\* and PCME++\* are identical, as they only model the variance of embeddings while keeping embedding directions constant, resulting in performance identical to the pre-trained models. In contrast, both AsymVLM and ProbVLM adapt the directions and learn the uncertainty of the embeddings during post-hoc training. Although ProbVLM achieves reasonable uncertainty estimates overall, it consistently underperforms pre-trained models in recall, whereas AsymVLM delivers richer uncertainty estimates and improves cross-modal retrieval performance.

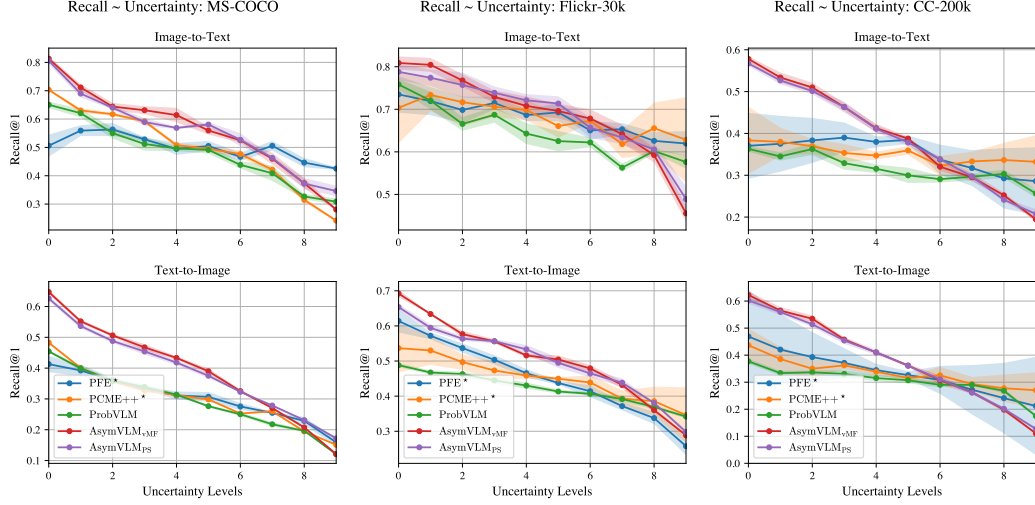


Figure 3: Recall@1 versus uncertainty levels for cross-modal retrieval tasks for various datasets. Each subplot shows the performance degradation as uncertainty increases for PFE\*, PCME++\*, ProbVLM, AsymVLM<sub>vMF</sub>, and AsymVLM<sub>PS</sub>. Ideally Recall@1 should decrease monotonically.

Table 1: Evaluation of model performance and uncertainty on benchmarks (MS-COCO, Flickr-30k, CC-200k) for Image-to-Text (i2t) and Text-to-Image (t2i) retrieval. We report Recall@1  $\uparrow$ , regression fit  $R^2 \uparrow$  between uncertainty and retrieval error, and Spearman’s rank  $S \downarrow$  correlation between uncertainty and retrieval error. **Bold** font denotes the best results and underline denotes the second best results. Each value is the mean of 5 runs with standard deviation in the Appendix, Table A.2.

DATASET	METHOD	T2I			I2T		
		Recall@1 $\uparrow$	$R^2 \uparrow$	$S \downarrow$	Recall@1 $\uparrow$	$R^2 \uparrow$	$S \downarrow$
MS-COCO	PFE*	0.500	0.558	-0.722	0.304	0.946	-0.988
	PCME++*	0.500	0.931	<b>-0.996</b>	0.304	0.948	-0.990
	ProbVLM	0.480	<b>0.951</b>	-0.981	0.293	0.979	<b>-1.000</b>
	AsymVLM <sub>vMF</sub>	<b>0.561</b>	0.948	-0.988	<b>0.392</b>	0.984	<b>-1.000</b>
	AsymVLM <sub>PS</sub>	<u>0.558</u>	0.937	-0.984	<u>0.390</u>	<b>0.989</b>	<b>-1.000</b>
FLICKR-30K	PFE*	0.680	0.675	-0.832	0.451	0.955	<b>-0.998</b>
	PCME++*	0.679	0.455	-0.178	0.451	0.900	-0.918
	ProbVLM	0.646	0.826	-0.914	0.422	<b>0.964</b>	-0.985
	AsymVLM <sub>vMF</sub>	<b>0.688</b>	<b>0.860</b>	<b>-0.976</b>	<b>0.504</b>	0.960	<u>-0.995</u>
	AsymVLM <sub>PS</sub>	<b>0.688</b>	<u>0.854</u>	-0.947	0.498	0.946	-0.993
CC-200K	PFE*	0.352	0.857	-0.521	0.336	0.988	-0.595
	PCME++*	0.352	0.198	-0.148	0.336	0.779	-0.887
	ProbVLM	0.316	0.772	-0.837	0.302	0.775	-0.965
	AsymVLM <sub>vMF</sub>	<b>0.395</b>	<u>0.990</u>	<b>-1.000</b>	<b>0.383</b>	<u>0.991</u>	-0.998
	AsymVLM <sub>PS</sub>	<u>0.393</u>	<b>0.992</b>	<b>-1.000</b>	<u>0.380</u>	<b>0.993</b>	<b>-1.000</b>

Furthermore, the similar performance of AsymVLM<sub>vMF</sub> and AsymVLM<sub>PS</sub> in both cross-modal retrieval and uncertainty quantification shows the robustness of AsymVLM w.r.t. the choice of the spherical distribution, suggesting possibilities of exploring other spherical or directional distributions.

## 5.2 Ablation study

We conduct an ablation study on the two important components of AsymVLM: the asymmetric architecture of the adapter, and the use of a spherical distribution for modeling. To assess the impact of two components, we designed following adapters with experimental results presented in Figure 4:

- **AsymVLM(image):** This variant modifies AsymVLM by only mapping deterministic image embeddings to spherical distributions, leaving text embeddings deterministic.
- **SymVLM:** This variant map both deterministic image and text embeddings to spherical distributions, with InfoNCE applied to symmetrized log likelihood kernel.

- **AsymVLM( $\mathcal{G}$ )**: This variant has identical architecture with AsymVLM but maps deterministic text embedding on Gaussian distribution, followed by normalization. The kernel of the loss function is replaced by Gaussian log likelihood.

**Asymmetric architecture** Both AsymVLM(image) and SymVLM perform worse than the original AsymVLM with respect to uncertainty quantification. Specifically, AsymVLM(image) struggles to model image uncertainty, showing no decrease in Recall@1 as uncertainty increases. Although SymVLM exhibits a slight decrease in Recall@1 with rising uncertainty, uncertainty estimates remain sub-optimal to AsymVLM. AsymVLM(image) achieves average Recall@1 comparable to AsymVLM while SymVLM performs much worse than either AsymVLM or AsymVLM(image). The results underscore the importance of an asymmetric architecture for uncertainty quantification and cross-modal retrieval performance.

**Choice of spherical distributions** For both Image-to-Text and Text-to-Image retrieval tasks, AsymVLM( $\mathcal{G}$ ) yields reasonable uncertainty estimates. As uncertainty levels increase, the Recall@1 of AsymVLM( $\mathcal{G}$ ) declines almost linearly, exhibiting behaviour similar to AsymVLM. However, the overall Recall@1 is inferior compared to AsymVLM. This emphasizes not only the effectiveness of the asymmetric architecture for uncertainty quantification, but also the necessity of spherical distributions for the post-hoc adaptation of pre-trained VLMs.

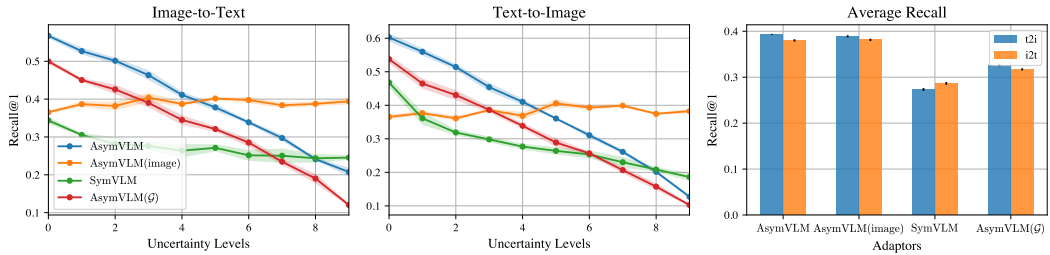


Figure 4: Ablation study results for AsymVLM: The left and middle panel shows Recall@1 performance for cross-modal retrieval across various uncertainty levels. The right panel summarizes average Recall@1 for both retrieval tasks.

### 5.3 Understanding the uncertainty estimates

To better understand the uncertainty estimates produced by AsymVLM, we analyze caption estimates on the HierarCap dataset. In this dataset, each image is paired with hierarchical captions spanning four levels – from general descriptions (Level 0) to detailed image descriptions (Level 3). Figure 5 illustrates the following observations.

- **AsymVLM captures hierarchical caption structure** Level 0 captions with general descriptions exhibit higher uncertainty estimates, indicating greater ambiguity, while Level 3 captions with the most detail generally show lower uncertainty. This pattern aligns with the inherent ambiguity of language and the corresponding uncertainty estimates provided by AsymVLM.
- **Detailed captions enhance image retrieval likelihood** The likelihood of the image embedding increases as more detailed descriptions are provided, as shown by the shift towards higher log likelihood values from Level 0 to 3. This suggests that detailed captions better capture the nuances of the image, facilitating more accurate image retrieval.
- **Longer captions exhibit reduced ambiguity** The results indicate that a higher token count is associated with lower uncertainty in the text, as depicted by the downward trend in uncertainty values. This is aligned with the expectation, as shorter texts generally tend to be more ambiguous, while longer captions provide more context, reducing ambiguity.

### 5.4 Applications

Below, we present two example applications of the uncertainty estimates obtained from AsymVLM, demonstrating their potential use cases.

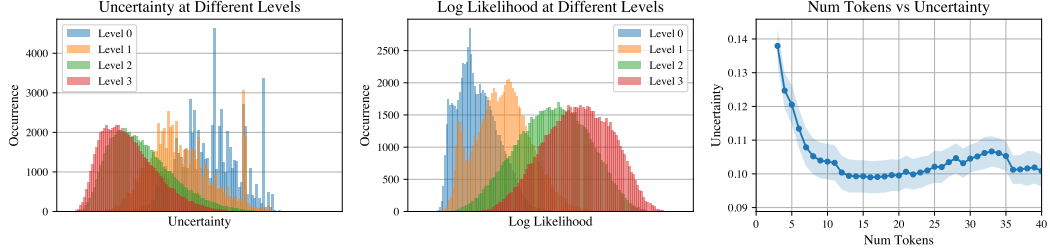


Figure 5: Uncertainty and likelihood analysis with the HierarCap dataset. The left panel shows the distribution of uncertainty estimates across hierarchical caption levels, showing decreasing uncertainty from Level 0 to 3. The middle panel illustrates the log likelihood distribution of image embeddings, with increased likelihood as caption detail increases. The right panel shows the relationship between the number of tokens and uncertainty, indicating reduced uncertainty with longer captions.

**Robust fine-tuning** Pre-trained VLMs are renowned for their zero-shot classification performance. However, fine-tuning these models on smaller datasets typically impairs this capability on other datasets. Table 2 compares AsymVLM with its deterministic counterpart, denoted by Determ.FT, and the foundation model without fine-tuning. Models fine-tuned with AsymVLM consistently outperform those fine-tuned deterministically across all settings. This suggests that AsymVLM preserves the zero-shot classification proficiency acquired during pre-training to a greater extent, whereas the deterministic approach is more prone to catastrophic forgetting. Therefore, AsymVLM offers a more robust fine-tuning strategy for VLMs.

**Handling none-of-the-above** For zero-shot classification, strategies to enable a model to say "none-of-the-above" rather than assigning an incorrect label include threshold-based rejection, margin-based rejection and other techniques. AsymVLM provides an alternative approach, by introducing a dummy prompt such as "a photo" to signal "none-of-the-above". We evaluate these methods on a combined test set consisting of CIFAR-10 and CIFAR-100 samples, performing zero-shot classification over CIFAR-10 classes. Ideally, CIFAR-10 samples (positive samples) should be correctly classified into their respective categories, while CIFAR-100 samples (negative samples) should be rejected as "none-of-the-above". AsymVLM consistently outperforms other methods (Table 3), achieving higher accuracy on both positive and negative samples.

Table 2: Zero-shot classification accuracy. "None" denotes the baseline without fine-tuning.

FINE-TUNED	METHOD	VALIDATED ON		
		CIFAR-10	CIFAR-100	STL-10
MS-COCO	Determ. FT	0.684	0.300	0.829
	AsymVLM <sub>PS</sub>	<b>0.847</b>	<u>0.470</u>	<b>0.952</b>
	AsymVLM <sub>VMF</sub>	<u>0.837</u>	<b>0.477</b>	<u>0.940</u>
FLICKR-30K	Determ. FT	0.688	0.342	0.874
	AsymVLM <sub>PS</sub>	<u>0.791</u>	<u>0.413</u>	<b>0.920</b>
	AsymVLM <sub>VMF</sub>	<b>0.792</b>	<u>0.422</u>	<u>0.918</u>
CC-200K	Determ. FT	0.779	0.411	0.922
	AsymVLM <sub>PS</sub>	<u>0.861</u>	<b>0.542</b>	<b>0.968</b>
	AsymVLM <sub>VMF</sub>	<b>0.866</b>	<u>0.542</u>	<u>0.967</u>
NONE	CLIP	0.888	0.642	0.974

Table 2: Zero-shot classification accuracy. "None" denotes the baseline without fine-tuning.

Table 3: None-of-the-above-aware zero-shot classification using dummy prompts. The table reports the accuracy on positive samples and negative samples.

DUMMY CLASS	METHOD	POS. ACC.	NEG. ACC.
"a photo"	CLIP	<b>0.888</b>	0.009
	Determ. FT	0.769	0.115
	AsymVLM <sub>PS</sub>	0.845	<u>0.547</u>
	AsymVLM <sub>VMF</sub>	<u>0.857</u>	<b>0.587</b>
"a photo of an object"	CLIP	<b>0.888</b>	0.009
	Determ. FT	0.778	0.037
	AsymVLM <sub>PS</sub>	0.849	<b>0.609</b>
	AsymVLM <sub>VMF</sub>	<u>0.858</u>	<u>0.557</u>
"a photo of something"	CLIP	<b>0.888</b>	0.009
	Determ. FT	0.769	0.125
	AsymVLM <sub>PS</sub>	0.843	<b>0.595</b>
	AsymVLM <sub>VMF</sub>	<u>0.857</u>	<u>0.585</u>
NONE	Margin-Based	0.584	0.579
	Threshold-Based	0.646	0.560

## 6 Conclusion and limitation

We introduced AsymVLM, a post-hoc probabilistic adaptation framework for pretrained vision–language models that leverages asymmetric uncertainty in textual and visual embeddings. Text embeddings are modeled as random variables using directional distributions (e.g., von Mises–Fisher

and power spherical) on the unit hypersphere, while image embeddings remain deterministic. Incorporating these spherical likelihoods into an InfoNCE-based objective enables effective modeling of wide-variance aleatoric uncertainty in language.

While AsymVLM delivers impressive performance in cross-modal retrieval with reliable uncertainty estimates, it only models text uncertainty. Future work could extend uncertainty modeling to image embeddings via data augmentation or similar methods. Also, although example applications of the uncertainty estimates are provided, further exploration into additional downstream tasks is warranted.

## Broader impact

Uncertainty estimates for text are vital in high-stakes applications involving VLMs, such as medical diagnostics where ambiguous language must be treated carefully. AsymVLM enhances trust in textual inputs, enabling safer and more robust applications of VLMs in uncertainty-sensitive domains.

## Acknowledgement

The computations/data handling were enabled by the Alvis resource provided by Alice Wallenberg Foundation at the National Supercomputer Centre and by the National Academic Infrastructure for Supercomputing in Sweden (NAIIS) at Chalmers e-Commons at Chalmers. LJ acknowledges funding from the Centre for Interdisciplinary Mathematics at Uppsala University and NAIIS through Project 2024/22-1358. AH and PS acknowledge support from the Swedish Research Council through grant agreement nos. 2023-05167 and 2023-05593 respectively. EV acknowledges support from the *Kjell & Märta Beijer* Foundation. PS also acknowledges support from the the Knut and Alice Wallenberg foundation through the Program for Academic leaders in Life Science (PALS).

## References

- [1] Rabab Abdelfattah, Qing Guo, Xiaoguang Li, Xiaofeng Wang, and Song Wang. Cdul: Clip-driven unsupervised learning for multi-label image classification. In *Proceedings of the IEEE/CVF International Conference on Computer Vision*, pages 1348–1357, 2023.
- [2] Morris Alper and Hadar Averbuch-Elor. Emergent visual-semantic hierarchies in image-text representations. In *European Conference on Computer Vision*, pages 220–238. Springer, 2024.
- [3] Anton Baumann, Rui Li, Marcus Klasson, Santeri Mentu, Shyamgopal Karthik, Zeynep Akata, Arno Solin, and Martin Trapp. Post-hoc probabilistic vision-language models. *arXiv preprint arXiv:2412.06014*, 2024.
- [4] Florian Bordes, Richard Yuanzhe Pang, Anurag Ajay, Alexander C Li, Adrien Bardes, Suzanne Petryk, Oscar Mañas, Zhiqiu Lin, Anas Mahmoud, Bargav Jayaraman, et al. An introduction to vision-language modeling. *arXiv preprint arXiv:2405.17247*, 2024.
- [5] Min Cao, Shiping Li, Juntao Li, Liqiang Nie, and Min Zhang. Image-text retrieval: A survey on recent research and development. *arXiv preprint arXiv:2203.14713*, 2022.
- [6] Ting Chen, Simon Kornblith, Mohammad Norouzi, and Geoffrey Hinton. A simple framework for contrastive learning of visual representations. In *International conference on machine learning*, pages 1597–1607. PMLR, 2020.
- [7] Xinlei Chen and Kaiming He. Exploring simple siamese representation learning. In *Proceedings of the IEEE/CVF conference on computer vision and pattern recognition*, pages 15750–15758, 2021.
- [8] Sanghyuk Chun, Seong Joon Oh, Rafael Sampaio De Rezende, Yannis Kalantidis, and Diane Larlus. Probabilistic embeddings for cross-modal retrieval. In *Proceedings of the IEEE/CVF Conference on Computer Vision and Pattern Recognition*, pages 8415–8424, 2021.
- [9] Adam Coates, Andrew Ng, and Honglak Lee. An analysis of single-layer networks in unsupervised feature learning. In *Proceedings of the fourteenth international conference on artificial intelligence and statistics*, pages 215–223. JMLR Workshop and Conference Proceedings, 2011.
- [10] Inderjit S Dhillon and Suvrit Sra. Modeling data using directional distributions. Technical report, Citeseer, 2003.
- [11] Minyoung Huh, Brian Cheung, Tongzhou Wang, and Phillip Isola. The platonic representation hypothesis. *CoRR*, 2024.
- [12] Alex Krizhevsky, Geoffrey Hinton, et al. Learning multiple layers of features from tiny images. 2009.
- [13] Junnan Li, Dongxu Li, Caiming Xiong, and Steven Hoi. Blip: Bootstrapping language-image pre-training for unified vision-language understanding and generation. In *International conference on machine learning*, pages 12888–12900. PMLR, 2022.
- [14] Tsung-Yi Lin, Michael Maire, Serge Belongie, James Hays, Pietro Perona, Deva Ramanan, Piotr Dollár, and C Lawrence Zitnick. Microsoft coco: Common objects in context. In *Computer Vision–ECCV 2014: 13th European Conference, Zurich, Switzerland, September 6–12, 2014, Proceedings, Part V 13*, pages 740–755. Springer, 2014.
- [15] Daniel W Lozier. Nist digital library of mathematical functions. *Annals of Mathematics and Artificial Intelligence*, 38:105–119, 2003.
- [16] Bryan A Plummer, Liwei Wang, Chris M Cervantes, Juan C Caicedo, Julia Hockenmaier, and Svetlana Lazebnik. Flickr30k entities: Collecting region-to-phrase correspondences for richer image-to-sentence models. In *Proceedings of the IEEE international conference on computer vision*, pages 2641–2649, 2015.

- [17] Alec Radford, Jong Wook Kim, Chris Hallacy, Aditya Ramesh, Gabriel Goh, Sandhini Agarwal, Girish Sastry, Amanda Askell, Pamela Mishkin, Jack Clark, et al. Learning transferable visual models from natural language supervision. In *International conference on machine learning*, pages 8748–8763. PMLR, 2021.
- [18] Diego Ruiz-Antolín and Javier Segura. A new type of sharp bounds for ratios of modified bessel functions. *Journal of Mathematical Analysis and Applications*, 443(2):1232–1246, 2016.
- [19] Mahtab Sandhu, Yann Batiste Pequignot, Samer B Nashed, Sabyasachi Sahoo, and Liam Paull. Clip-enhance: Improving clip zero-shot classification via von mises-fisher clustering. 2025.
- [20] Tyler R Scott, Andrew C Gallagher, and Michael C Mozer. von mises-fisher loss: An exploration of embedding geometries for supervised learning. In *Proceedings of the IEEE/CVF international conference on computer vision*, pages 10612–10622, 2021.
- [21] Philip Sedgwick. Spearman’s rank correlation coefficient. *Bmj*, 349, 2014.
- [22] Piyush Sharma, Nan Ding, Sebastian Goodman, and Radu Soricut. Conceptual captions: A cleaned, hypernymed, image alt-text dataset for automatic image captioning. In *Proceedings of the 56th Annual Meeting of the Association for Computational Linguistics (Volume 1: Long Papers)*, pages 2556–2565, 2018.
- [23] Yichun Shi and Anil K Jain. Probabilistic face embeddings. In *Proceedings of the IEEE/CVF international conference on computer vision*, pages 6902–6911, 2019.
- [24] Uddeshya Upadhyay, Shyamgopal Karthik, Massimiliano Mancini, and Zeynep Akata. Probvlm: Probabilistic adapter for frozen vision-language models. In *Proceedings of the IEEE/CVF International Conference on Computer Vision*, pages 1899–1910, 2023.
- [25] Tongzhou Wang and Phillip Isola. Understanding contrastive representation learning through alignment and uniformity on the hypersphere. In Hal Daumé III and Aarti Singh, editors, *Proceedings of the 37th International Conference on Machine Learning*, volume 119 of *Proceedings of Machine Learning Research*, pages 9929–9939. PMLR, 13–18 Jul 2020.
- [26] Haoran Wei, Lingyu Kong, Jinyue Chen, Liang Zhao, Zheng Ge, Jinrong Yang, Jianjian Sun, Chunrui Han, and Xiangyu Zhang. Vary: Scaling up the vision vocabulary for large vision-language model. In *European Conference on Computer Vision*, pages 408–424. Springer, 2025.
- [27] Linda Wetzel. *Types and tokens: On abstract objects*. MIT press, 2009.
- [28] Xiaohua Zhai, Basil Mustafa, Alexander Kolesnikov, and Lucas Beyer. Sigmoid loss for language image pre-training. In *Proceedings of the IEEE/CVF International Conference on Computer Vision*, pages 11975–11986, 2023.
- [29] Jingyi Zhang, Jiaxing Huang, Sheng Jin, and Shijian Lu. Vision-language models for vision tasks: A survey. *IEEE Transactions on Pattern Analysis and Machine Intelligence*, 2024.

## A Method Details

### A.1 Approximation of the log normalizer of vMF distribution

The normalizer of vMF distribution  $C_d(\kappa)$  is given by,

$$C_d(\kappa) = \frac{\kappa^{d/2-1}}{(2\pi)^{d/2} I_{d/2-1}(\kappa)}.$$

**Remark 1** (Derivatives of modified Bessel functions [15]). *Let  $I_v(z)$  denote modified Bessel function of  $v$ -th order. For  $k = 0, 1, 2, \dots$ ,*

$$\left(\frac{1}{z} \frac{d}{dz}\right)^k (z^v I_v(z)) = z^{v-k} I_{v-k}(z).$$

**Lemma 1.** *The first order derivate of  $I_v(z)$  is,*

$$\frac{d}{dz} I_v(z) = I_{v+1}(z) + \frac{v}{z} I_v(z).$$

*Proof.* Using Remark 1, let  $k = 1$  and we have,

$$\begin{aligned} \frac{1}{z} \frac{d}{dz} z^v I_v(z) &= z^{v-1} I_{v-1}(z), \\ v z^{v-1} I_v(z) + z^v \frac{dI_v(z)}{dz} &= z^v I_{v-1}(z). \end{aligned}$$

Reorganizing the equation gives us,

$$\frac{d}{dz} I_v(z) = I_{v-1}(z) - \frac{v}{z} I_v(z).$$

Further we use the Recurrence Relations of modified Bessel function [15],

$$I_{v-1}(z) - I_{v+1}(z) = \frac{2v}{z} I_v(z),$$

and obtain,

$$\frac{d}{dz} I_v(z) = I_{v+1}(z) + \frac{v}{z} I_v(z).$$

□

Note that,

$$\begin{aligned} \frac{d}{d\kappa} \ln C_d(\kappa) &= \frac{d}{d\kappa} \left[ (d/2 - 1) \ln \kappa - d/2 \ln 2\pi - \ln I_{d/2-1}(\kappa) \right], \\ &= \frac{d/2 - 1}{\kappa} - \frac{dI_{d/2-1}(\kappa)/d\kappa}{I_{d/2-1}(\kappa)}. \end{aligned}$$

Using Lemma 1, we have,

$$\begin{aligned} \frac{d}{d\kappa} \ln C_d(\kappa) &= \frac{d/2 - 1}{\kappa} - \frac{I_{d/2}(\kappa) + \frac{d/2-1}{\kappa} I_{d/2-1}(\kappa)}{I_{d/2-1}(\kappa)}, \\ &= -\frac{I_{d/2}(\kappa)}{I_{d/2-1}(\kappa)}. \end{aligned}$$

Ruiz-Antolín and Segura [18] give a tight lower and upper bound for  $-\frac{I_{d/2}(\kappa)}{I_{d/2-1}(\kappa)}$ , given by following Remark:

**Remark 2** (Tight lower and upper bound for the ratio of modified Bessel functions [18]). Let  $I_v(z)$  be the modified Bessel function of the first kind at order  $v$ . We have following bound,

$$\frac{z}{v - 1/2 + \sqrt{(v + 1/2)^2 + z^2}} < \frac{I_v(z)}{I_{v-1}(z)} < \frac{z}{v - 1/2 + \sqrt{(v - 1/2)^2 + z^2}}, v \geq 1/2.$$

With the tight lower and upper bounds,  $\frac{I_v(z)}{I_{v-1}(z)}$  can be approximated by,

$$\frac{I_v(z)}{I_{v-1}(z)} \approx \frac{1}{2}(g(z) + h(z)),$$

where  $g(z)$  and  $h(z)$  denote the left and right hand sides of the inequality.

To further approximate  $\ln C_d(\kappa)$ , by plugging  $v = \frac{d}{2}$ , we further integrate the function w.r.t  $\kappa$ , and obtain following approximates,

$$\begin{aligned} \ln C_d(\kappa) &\approx \frac{d-1}{4} \ln \left( \frac{d-1}{2} + \sqrt{\left( \frac{d-1}{2} \right)^2 + \kappa^2} \right) - \frac{1}{2} \sqrt{\left( \frac{d-1}{2} \right)^2 + \kappa^2} \\ &\quad + \frac{d-1}{4} \ln \left( \frac{d-1}{2} + \sqrt{\left( \frac{d+1}{2} \right)^2 + \kappa^2} \right) - \frac{1}{2} \sqrt{\left( \frac{d+1}{2} \right)^2 + \kappa^2} + \text{const.} \end{aligned} \quad (4)$$

## A.2 Inference with maximum log likelihood

The inference of deterministic pre-trained VLMs (i.e. cross-modal retrieval) relies on computing the cosine similarities of each possible pairs of given texts and images, while the inference for AsymVLM has a clear statistical interpretation as maximizing log likelihood w.r.t. different image-text pairs. For Image-to-Text retrieval, given a set of text embeddings  $\{\mathbf{z}_r^T | r \in [R]\}$ , where  $\mathbf{z}_r^T \sim \text{vMF}(\mu(t_r), \kappa(t_r))$  or  $\mathbf{z}_r^T \sim \text{PS}(\mu(t_r), \kappa(t_r))$ , and an image embeddings  $\mathbf{z}^I$ , the predictor is given by,

$$\hat{r} = \arg \max_{r \in [R]} \ln p_{\mathbf{z}_r^T}(\mathbf{z}^I) = \begin{cases} \kappa(t_r) \cdot (\mu(t_r))^\top \mathbf{z}^I + F_d(\kappa(t_r)) & \text{for vMF,} \\ \kappa(t_r) \ln(1 + (\mu(t_r))^\top \mathbf{z}^I) + \ln C_d(\kappa(t_r)) & \text{for PS.} \end{cases}$$

Similarly, for Text-to-Image retrieval, given a set of image embeddings  $\{\mathbf{z}_s^I | s \in [S]\}$  and a text embedding  $\mathbf{z}^T \sim \text{vMF}(\mu, \kappa)$  or  $\mathbf{z}^T \sim \text{PS}(\mu, \kappa)$ , the predictor is given by,

$$\hat{s} = \arg \max_{s \in [S]} \ln p_{\mathbf{z}_s^I}(\mathbf{z}^T) = \begin{cases} \kappa \cdot \mu^\top \mathbf{z}_s^I + F_d(\kappa) & \text{for vMF,} \\ \kappa \ln(1 + \mu^\top \mathbf{z}_s^I) + \ln C_d(\kappa) & \text{for PS.} \end{cases}$$

## A.3 Derivation for the SigLIP variant

The objective function of SigLIP is defined as,

$$-\frac{1}{B} \sum_{r=1}^B \sum_{s=1}^B \ln \frac{1}{1 + \exp(\sigma(r, s)(-\tau \cdot \text{CosSim}(r, s) + b))},$$

where  $\sigma(r, s) = 1$  if  $r = s$  and  $\sigma(r, s) = -1$  if  $r \neq s$ . SigLIP shares the identical "kernel", i.e. cosine similarity, with CLIP, while our methods employs different kernels with variance modeling derived from vMF/PS assumptions for the text embeddings. By replacing the kernel of the objective function of SigLIP, we can also obtain the SigLIP variant of our method.

## B Experimental Protocol

### B.1 Adapter architecture

The text adapter is implemented as a three-layer perceptron that takes the output of a pre-trained text encoder as its input. It consists of two hidden layers, each with 512 dimensions and activated

by the ReLU function, followed by an output layer that has the same dimensionality as the input, and no activation function. Batch normalization is applied to all layers to stabilize training. The un-normalized output of the final layer, denoted as  $z'_t$ , is decomposed into  $z'_t = \kappa \mu_t$ , where the vector  $\|\mu_t\| = 1$  and the scalar  $\kappa > 0$ , serving as the parameters for either vMF or PS distribution. The temperature parameter in the InfoNCE objective function is trainable.

Other adapters (ProbVLM, PFE\* and PCME++\*) share identical architectures as three-layer perceptron, with different number of outputs for the last layer due to the inherent different parameterization in the methods.

## B.2 Datasets

We use the datasets MS-COCO and Flickr-30k to train and validate the adapters since they provide well-annotated image–caption pairs. Additionally, we randomly sample 200k image-caption pairs from Conceptual Caption dataset [22], building a dataset (CC-200k) for the training and validation. For ablation studies, all methods are trained on the training set of CC-200k and evaluated on the validation set of CC-200k. For the study of understanding the learned uncertainty, the model is evaluated on HierarCap dataset [2], a dataset adapted from Conceptual Caption to reflect the hierarchical structure of captions. For each image, there exists four captions of different abstraction levels from general to detailed ones. For example applications, CIFAR-10, CIFAR-100 [12] and STL10 [9] are used for zero-shot classification.

**Metrics** The evaluation of the quality of aleatoric uncertainty / ambiguity estimates for text embeddings is based on the recall performance in cross-modal retrieval tasks. A strong positive correlation between uncertainty and error indicates that when the model is more uncertain, it tends to produce lower-quality embeddings, which leads to poorer retrieval performance. For each task, we first group the recall results according to the uncertainty levels of the text embeddings. Then we compare Spearman’s rank correlation ( $S$ ) between the uncertainty levels and recall for cross-modal retrieval [21]. We also compute the regression fit  $R^2$  between the uncertainty levels and Recall@1 performances to measure if the drop in performance follows a linear trend. To evaluate the overall performance of cross-modal retrieval of the models trained with different methods, we also compare the average Recall@1 across all uncertainty levels.

## B.3 Baseline methods

The uncertainty quantification baselines include ProbVLM, PFE and PCME++ adapted/trained in a post-hoc manner from pretrained models (denoted by PFE\* and PCME++\*, respectively). Note that the post-hoc adaptation for both PFE and PCME++ only predicts the variances of probabilistic embeddings, while keeping the means unchanged from the pretrained models. This is due to PFE and PCME++ achieving poor performance (worse than pre-trained models) for cross-modal retrieval, when used to adapt the means of the embeddings. For downstream tasks, vanilla pre-trained vision-language models are also included. BayesVLM is not compared against with other methods in the main experiments, as it does not provide a single scalar value quantifying the uncertainty of its embeddings, rather scalar uncertainty for cosine similarities propagated by probabilistic embeddings.

## B.4 Optimization protocol

All methods are implemented in PyTorch, and all pre-trained VLMs are loaded by `transformers`. All computations are conducted on NVIDIA A100/A40 GPUs. We use stochastic gradient descent with momentum (SGD-momen.) for the optimization of AsymVLM, PCME and PFE, and use AdamW for ProbVLM, following its official implementation. The learning rates for different methods are optimized using a grid search within  $\{10^{-4}, 5 \times 10^{-4}, 10^{-3}, 5 \times 10^{-3}, 10^{-2}, 5 \times 10^{-2}\}$ , and reported as Table A.1. We apply cosine annealing for learning rate scheduling with a minimal learning rate  $10^{-6}$ .

## C Supplementary Empirical Results

Complete experimental results for the evaluation of AsymVLM on CLIP embeddings are presented in Table A.2 (mean  $\pm$  std. dev. over 5 runs).

Table A.1: Optimizer configurations for different methods

Method	Optimizer	Learning rate	Batch size
AsymVLM	SGD	$10^{-2}$	2048
ProbVLM	AdamW	$10^{-4}$	2048
PFE*	SGD	$10^{-3}$	2048
PCME++*	SGD	$5 \times 10^{-4}$	2048

Table A.2: Complete experimental results for the comparison of different methods for CLIP embeddings.

DATASET	METHOD	I2T			T2I		
		Recall@1 $\uparrow$	$R^2 \uparrow$	$S \downarrow$	Recall@1 $\uparrow$	$R^2 \uparrow$	$S \downarrow$
MS-COCO	PFE*	0.500 $\pm$ 0.000	0.558 $\pm$ 0.253	-0.722 $\pm$ 0.193	0.304 $\pm$ 0.000	0.946 $\pm$ 0.021	-0.988 $\pm$ 0.008
	PCME++*	0.500 $\pm$ 0.000	0.931 $\pm$ 0.006	<b>-0.996 <math>\pm</math> 0.004</b>	0.304 $\pm$ 0.000	0.948 $\pm$ 0.010	-0.990 $\pm$ 0.004
	ProbVLM	0.480 $\pm$ 0.004	<b>0.951 <math>\pm</math> 0.011</b>	-0.981 $\pm$ 0.006	0.293 $\pm$ 0.001	0.979 $\pm$ 0.002	<b>-1.000 <math>\pm</math> 0.000</b>
	AsymVLM <sub>VMF</sub>	<b>0.561 <math>\pm</math> 0.002</b>	0.948 $\pm$ 0.016	<u>0.988 <math>\pm</math> 0.013</u>	<b>0.392 <math>\pm</math> 0.001</b>	0.984 $\pm$ 0.004	<b>-1.000 <math>\pm</math> 0.000</b>
	AsymVLM <sub>PS</sub>	0.558 $\pm$ 0.004	0.937 $\pm$ 0.013	-0.984 $\pm$ 0.012	0.390 $\pm$ 0.002	<b>0.989 <math>\pm</math> 0.001</b>	<b>-1.000 <math>\pm</math> 0.000</b>
FLICKR-30K	PFE*	0.680 $\pm$ 0.000	0.675 $\pm$ 0.186	-0.832 $\pm$ 0.094	0.451 $\pm$ 0.000	0.955 $\pm$ 0.002	<b>-0.998 <math>\pm</math> 0.005</b>
	PCME++*	0.679 $\pm$ 0.001	0.455 $\pm$ 0.386	-0.178 $\pm$ 0.650	0.451 $\pm$ 0.000	0.900 $\pm$ 0.063	-0.918 $\pm$ 0.067
	ProbVLM	0.646 $\pm$ 0.006	0.826 $\pm$ 0.062	-0.914 $\pm$ 0.029	0.422 $\pm$ 0.002	<b>0.964 <math>\pm</math> 0.016</b>	-0.985 $\pm$ 0.012
	AsymVLM <sub>VMF</sub>	<b>0.688 <math>\pm</math> 0.005</b>	<b>0.860 <math>\pm</math> 0.029</b>	<b>-0.976 <math>\pm</math> 0.010</b>	<b>0.504 <math>\pm</math> 0.001</b>	0.960 $\pm$ 0.006	<b>-0.995 <math>\pm</math> 0.006</b>
	AsymVLM <sub>PS</sub>	<b>0.688 <math>\pm</math> 0.005</b>	0.854 $\pm$ 0.021	-0.947 $\pm$ 0.032	0.498 $\pm$ 0.002	0.946 $\pm$ 0.021	-0.993 $\pm$ 0.006
CC-200K	PFE*	0.352 $\pm$ 0.000	0.857 $\pm$ 0.075	-0.521 $\pm$ 0.757	0.336 $\pm$ 0.000	0.988 $\pm$ 0.008	-0.595 $\pm$ 0.798
	PCME++*	0.352 $\pm$ 0.000	0.198 $\pm$ 0.375	-0.148 $\pm$ 0.430	0.336 $\pm$ 0.000	0.779 $\pm$ 0.105	-0.887 $\pm$ 0.060
	ProbVLM	0.316 $\pm$ 0.001	0.772 $\pm$ 0.102	-0.837 $\pm$ 0.066	0.302 $\pm$ 0.001	0.775 $\pm$ 0.029	-0.965 $\pm$ 0.021
	AsymVLM <sub>VMF</sub>	<b>0.395 <math>\pm</math> 0.002</b>	0.990 $\pm$ 0.003	<b>-1.000 <math>\pm</math> 0.000</b>	<b>0.383 <math>\pm</math> 0.003</b>	0.991 $\pm$ 0.002	<b>-0.998 <math>\pm</math> 0.005</b>
	AsymVLM <sub>PS</sub>	0.393 $\pm$ 0.001	<b>0.992 <math>\pm</math> 0.004</b>	<b>-1.000 <math>\pm</math> 0.000</b>	<u>0.380 <math>\pm</math> 0.002</u>	<b>0.993 <math>\pm</math> 0.001</b>	<b>-1.000 <math>\pm</math> 0.000</b>

Complete experimental results for the evaluation of AsymVLM on SigLip embeddings are presented in Table A.3.

Table A.3: Full experimental results for the comparison of different methods for SigLip embeddings.

DATASET	METHOD	I2T			T2I		
		Recall@1 $\uparrow$	$R^2 \uparrow$	$S \downarrow$	Recall@1 $\uparrow$	$R^2 \uparrow$	$S \downarrow$
MS-COCO	PFE*	0.654 $\pm$ 0.000	<b>0.940 <math>\pm</math> 0.010</b>	-0.990 $\pm$ 0.005	0.472 $\pm$ 0.000	<b>0.996 <math>\pm</math> 0.001</b>	<b>-1.000 <math>\pm</math> 0.000</b>
	PCME++*	0.654 $\pm$ 0.000	0.021 $\pm$ 0.016	-0.101 $\pm$ 0.020	0.472 $\pm$ 0.000	0.893 $\pm$ 0.016	-0.907 $\pm$ 0.031
	ProbVLM	0.649 $\pm$ 0.001	0.564 $\pm$ 0.063	-0.672 $\pm$ 0.064	0.469 $\pm$ 0.001	0.935 $\pm$ 0.007	-0.998 $\pm$ 0.005
	AsymVLM <sub>VMF</sub>	<b>0.694 <math>\pm</math> 0.002</b>	<b>0.948 <math>\pm</math> 0.018</b>	<b>-0.995 <math>\pm</math> 0.006</b>	<b>0.502 <math>\pm</math> 0.000</b>	0.986 $\pm$ 0.001	<b>-1.000 <math>\pm</math> 0.000</b>
	AsymVLM <sub>PS</sub>	0.691 $\pm$ 0.002	0.929 $\pm$ 0.021	-0.993 $\pm$ 0.015	0.497 $\pm$ 0.001	<b>0.987 <math>\pm</math> 0.002</b>	<b>-1.000 <math>\pm</math> 0.000</b>
FLICKR-30K	PFE*	0.815 $\pm$ 0.000	<b>0.840 <math>\pm</math> 0.023</b>	-0.947 $\pm$ 0.030	0.638 $\pm$ 0.000	0.922 $\pm$ 0.005	<b>-0.998 <math>\pm</math> 0.005</b>
	PCME++*	0.814 $\pm$ 0.000	0.007 $\pm$ 0.002	0.127 $\pm$ 0.070	0.638 $\pm$ 0.000	0.472 $\pm$ 0.016	-0.625 $\pm$ 0.027
	ProbVLM	0.807 $\pm$ 0.002	0.519 $\pm$ 0.097	-0.714 $\pm$ 0.119	0.631 $\pm$ 0.000	0.525 $\pm$ 0.038	-0.640 $\pm$ 0.151
	AsymVLM <sub>VMF</sub>	<b>0.823 <math>\pm</math> 0.002</b>	0.803 $\pm$ 0.044	<b>-0.967 <math>\pm</math> 0.010</b>	0.647 $\pm$ 0.001	0.934 $\pm$ 0.010	<b>-0.998 <math>\pm</math> 0.005</b>
	AsymVLM <sub>PS</sub>	0.819 $\pm$ 0.006	<b>0.891 <math>\pm</math> 0.024</b>	-0.959 $\pm$ 0.012	<b>0.649 <math>\pm</math> 0.002</b>	<b>0.949 <math>\pm</math> 0.008</b>	<b>-0.998 <math>\pm</math> 0.005</b>
CC-200K	PFE*	0.503 $\pm$ 0.000	0.981 $\pm$ 0.003	<b>-1.000 <math>\pm</math> 0.000</b>	0.484 $\pm$ 0.000	<b>0.992 <math>\pm</math> 0.004</b>	<b>-1.000 <math>\pm</math> 0.000</b>
	PCME++*	0.502 $\pm$ 0.000	0.933 $\pm$ 0.009	-0.956 $\pm$ 0.010	0.484 $\pm$ 0.000	0.889 $\pm$ 0.016	-0.965 $\pm$ 0.014
	ProbVLM	0.489 $\pm$ 0.002	0.674 $\pm$ 0.081	-0.817 $\pm$ 0.071	0.477 $\pm$ 0.000	0.744 $\pm$ 0.022	-0.934 $\pm$ 0.029
	AsymVLM <sub>VMF</sub>	<b>0.516 <math>\pm</math> 0.002</b>	<b>0.991 <math>\pm</math> 0.004</b>	<b>-1.000 <math>\pm</math> 0.000</b>	<b>0.496 <math>\pm</math> 0.002</b>	<b>0.993 <math>\pm</math> 0.002</b>	<b>-1.000 <math>\pm</math> 0.000</b>
	AsymVLM <sub>PS</sub>	0.514 $\pm$ 0.001	0.984 $\pm$ 0.003	<b>-1.000 <math>\pm</math> 0.000</b>	0.489 $\pm$ 0.002	0.985 $\pm$ 0.002	<b>-1.000 <math>\pm</math> 0.000</b>

Complete experimental results for the evaluation of AsymVLM for robust out-of-distribution zero-shot classification are presented in Table A.4.

Complete experimental results for the evaluation of AsymVLM for zero-shot classification, with none-of-the-above handling are presented in Table A.5.

Table A.4: Full experimental results for Out-of-distribution zero-shot classification accuracy on CIFAR-10, CIFAR-100 and STL-10 for pretrained VLMs fine-tuned with different methods on MS-COCO, Flickr-30k and CC-200k datasets.

FINE-TUNED ON	METHOD	VALIDATED ON		
		CIFAR-10	CIFAR-100	STL-10
MS-COCO	Determ. FT	0.684 $\pm$ 0.055	0.300 $\pm$ 0.017	0.829 $\pm$ 0.030
	AsymVLM <sub>PS</sub>	<b>0.847 <math>\pm</math> 0.007</b>	<u>0.470 <math>\pm</math> 0.012</u>	<b>0.952 <math>\pm</math> 0.005</b>
	AsymVLM <sub>VMF</sub>	<u>0.837 <math>\pm</math> 0.010</u>	<b>0.477 <math>\pm</math> 0.010</b>	<u>0.940 <math>\pm</math> 0.010</u>
FLICKR-30K	Determ. FT	0.688 $\pm$ 0.030	0.342 $\pm$ 0.019	0.874 $\pm$ 0.012
	AsymVLM <sub>PS</sub>	<u>0.791 <math>\pm</math> 0.019</u>	<u>0.413 <math>\pm</math> 0.009</u>	<b>0.920 <math>\pm</math> 0.009</b>
	AsymVLM <sub>VMF</sub>	<b>0.792 <math>\pm</math> 0.011</b>	<b>0.422 <math>\pm</math> 0.014</b>	<u>0.918 <math>\pm</math> 0.006</u>
CC-200K	Determ. FT	0.779 $\pm$ 0.037	0.411 $\pm$ 0.011	0.922 $\pm$ 0.017
	AsymVLM <sub>PS</sub>	<u>0.861 <math>\pm</math> 0.008</u>	<b>0.542 <math>\pm</math> 0.005</b>	<b>0.968 <math>\pm</math> 0.001</b>
	AsymVLM <sub>VMF</sub>	<b>0.866 <math>\pm</math> 0.013</b>	<b>0.542 <math>\pm</math> 0.013</b>	<u>0.967 <math>\pm</math> 0.004</u>
NONE	CLIP	0.888	0.642	0.974

Table A.5: Complete results for the evaluation metrics for various zero-shot classification methods using different dummy prompts. The table reports the accuracy on positive samples and negative samples when classifying all inputs into CIFAR-10 classes. Baseline methods using threshold- and margin-based rejection are included for comparison.

DUMMY PROMPT	METHOD	POSITIVE ACC.	NEGATIVE ACC.
"a photo"	CLIP	<b>0.888</b>	0.009
	Determ. FT	0.769 $\pm$ 0.028	0.115 $\pm$ 0.138
	AsymVLM <sub>PS</sub>	0.845 $\pm$ 0.011	<u>0.547 <math>\pm</math> 0.106</u>
	AsymVLM <sub>VMF</sub>	<u>0.857 <math>\pm</math> 0.010</u>	<b>0.587 <math>\pm</math> 0.110</b>
"a photo of an object"	CLIP	<b>0.888</b>	0.009
	Determ. FT	0.778 $\pm$ 0.040	0.037 $\pm$ 0.026
	AsymVLM <sub>PS</sub>	0.849 $\pm$ 0.012	<b>0.609 <math>\pm</math> 0.119</b>
	AsymVLM <sub>VMF</sub>	0.858 $\pm$ 0.011	<u>0.557 <math>\pm</math> 0.089</u>
"a photo of something"	CLIP	<b>0.888</b>	0.009
	Determ. FT	0.769 $\pm$ 0.031	0.125 $\pm$ 0.132
	AsymVLM <sub>PS</sub>	0.843 $\pm$ 0.019	<b>0.595 <math>\pm</math> 0.149</b>
	AsymVLM <sub>VMF</sub>	<u>0.857 <math>\pm</math> 0.009</u>	<u>0.585 <math>\pm</math> 0.107</u>
NONE	Margin-Based	0.584	0.579
	Threshold-Based	0.646	0.560